Investigating the Decay Amplitude Models Based on Dalitz Plot Analysis for $B^0 \to K^+\pi^-\pi^0$ Decays
Untersuchung der Zerfallsamplitudenmodelle basierend auf der Dalitz-Plot-Analyse für $B^0 \to K^+\pi^-\pi^0$ Zerfälle

Department of Physics
Ludwig-Maximilians-Universität München

Ceren Ay

Munich, February 5$^{\mathrm{th}}$, 2025

Supervised by Prof. Dr. Thomas Kuhr, Dr. Stefan Wallner

Abstract

Amplitude calculations are essential tools for understanding the underlying physics. These measurements are particularly challenging for the decays of B mesons to multi-body hadronic final states, since elaborate amplitude analyses are required to separate and measure the contributions of the interfering resonances in these final states. We perform a Dalitz plot analysis of data recorded by the Belle II experiment to extract these parameters for $B^0 \to K^+\pi^-\pi^0$ decays. As part of this, we investi- gate the model dependence by studying different parameterizations of amplitude models. We also check the dependence on the initial values of the fit and investigate fit biases.

Contents

1 Introduction

Understanding the fundamental properties of particle decays is essential in exploring the nature of subatomic interactions and testing the limits of the Standard Model (SM). One of the key attributes in studying particle decays is the amplitude of the decay process, which encodes the probability of different possible decay mode. By analyzing these amplitudes, we can determine whether our theoretical description of a decay is complete or if there are missing contributions, potentially indicating the presence of new physics. However the theoretical determination of the amplitudes is challenging, especially when processes from quantum chromodynamics (QCD) is involved. Often, they are done based on approximations which give way to multiple models with various parametrizations.
In this study, we focus on the amplitude models of $B^0 \to K^+\pi^-\pi^0$, a charmless hadronic B^0 decay. These decays are particularly interesting because they are suppressed at the tree level within the Cabibbo-Kobayashi-Maskawa (CKM) framework and are dominated by loop-level transitions. This suppression makes them sensitive probes for potential contributions from physics beyond the Standard Model, as new particles could appear virtually in these loop diagrams and small effects are more visible because SM physics suppressed. Nevertheless, the theoretical description of such decays is challenging due to the complex hadronic matrix elements of QCD that govern their internal structure.
One method that can be used to determine the amplitude is the Dalitz plot formalism, where interferences of the intermediate resonances are 'detangled', and the amplitude is expressed as a sum of the individual Amplitudes of each resonance with different weights. The experimental calculation we use for the the decay amplitude is based on this formalism, where we fit data to determine the complex coefficients, i. e. the weights, of each resonance contributing to the decay.
In the following chapters, we will first provide an overview of the decay process and its theoretical implications. Next, we will introduce the amplitude models used to describe the decay and then explain why we use the Dalitz plot formalism. We will continue with explaining the components of the Amplitude described by this formalism and discuss different parametrization choices and their impact. Then we will show our analysis for the model with different parametrizations. But, before we present our computational approach for determining the amplitude, we will evaluate the performance of the fitter we use for extracting the complex coefficients. Finally, we will talk abou the results and discuss the next steps. Through this analysis, we aim to deepen our understanding of charmless B^0 decays and the explore the relation between the theoretical and experimental determinations of the amplitude to describe the decay process of the $B^0 \to K^+\pi^-\pi^0$.

2 Theory

2.1 B meson

The name meson, described by particle physics, refers to the category of hadrons containing an equal number of quarks and antiquarks. A B meson is then described as a particle consisting of a bottom antiquark paired with either an up, down, strange, or charm quark. These bound states are classified as $B_u(B^+), B_d(B^0), B_s(B_s^0)$, and $B_c(B_c^+)$ mesons, depending on the accompanying quark type. The bottom quark is part of the third generation of quarks as the weak-doublet partner of the top quark. The existence of the third–generation quark doublet was proposed in 1973 by Kobayashi and Maskawa in their model of the quark mixing matrix ("CKM" matrix) [1], and confirmed four years later by the first observation of a $b\bar{b}$ meson. [2].

2.2 B decays

The B meson has various decays such as leptonic decays, in which the quarks of the decaying hadron annihilate each other and only leptons appear in the final state; semileptonic decays, in which both leptons and hadrons appear in the final state; or hadronic decays, in which the final state consists of hadrons only.

Charmless B decays

B-mesons can decay into particles that do not include any charm quarks. These decays are known as charmless hadronic B-meson decays. Since the b quark is much lighter than top quark, b quark then must transition into an up, down, or strange quark when we exclude the charm quarks. The decay products of charmless hadronic B-meson decays typically are pions and kaons, which are mesons composed of up and down quarks, and strange and up or down quarks, respectively. We look at $B^0 \to K^+\pi^-\pi^0$.

2.3 Dalitz Plot Analysis

Unlike two body decays where the energies of the final state particles are fully determined by the conservation of energy and momentum, three body decays have five dimensional phase space after imposing energy and momentum conservation. In the case where the initial and final state particles all have spin zero, after taking into account arbitrary rotations, the dimension of the phase space reduces to 2. If we describe the the three-body decay as

$$\overline{B}(p_B) \to M_a(p_1)M_b(p_2)M_c(p_3),$$

and fix the masses of the initial and final hadrons, the kinematics can be completely specified by two invariant masses of two pairs of final state particles.

2.3.1 Parametrization of Dalitz Plots

There is freedom in the choice of which two variables one uses to describe the amplitude of a three-body decay. It is often convenient to choose a pair of variables where the phase-space term is constant within the kinematically allowed region in the two-dimensional space spanned by these variables, resulting a more apparent structure of the amplitude. This can be achieved by taking either the kinetic energies of two of the final-state particles, or the squares of the invariant masses of two pairs of final-state particles. The parametrization using the squares of the invariant masses of two pairs of final-state particles is generally more suitable for relativistic decays and has an advantage of allowing easy determination of the masses of the intermediate states.

2.3.2 The Kinematic Boundaries

The invariant masses of pairs of final-state particles have the relation:

$$m_{12}^2 + m_{23}^2 + m_{13}^2 = M^2 + m_1^2 + m_2^2 + m_3^2 \tag{1}$$

The range of invariant masses m_{bc}^2 can be written in terms of either one of the other squared invariant masses. The Dalitz plot variable m_{12}^2 is kinematically limited by

$$m_{12,\,\mathrm{min}}^2 = (m_1 + m_2)^2, \tag{2}$$

and

$$m_{12,\,\mathrm{max}}^2 = (m_B - m_3)^2, \tag{3}$$

where $m_{12,\,\mathrm{min}}^2$ is the case when the whole kinematic energy is carried by particle 3 and the 12 system is at rest, and $m_{12,\,\mathrm{max}}^2$ is the when where particle 3 is at rest and all kinematic energy carried by the 12 system.
For a given m_{12}^2, m_{23}^2 is then limited by

$$m_{23,\,\mathrm{min}}^2(m_{12}) = \left(E_2^{12}(m_{12}) + E_3^{12}(m_{12})\right)^2 - \left(\sqrt{E_2^{12}(m_{12})^2 - m_2^2} + \sqrt{E_3^{12}(m_{12})^2 - m_3^2}\right)^2, \tag{4}$$

$$m_{23,\,\mathrm{max}}^2(m_{12}) = \left(E_2^{12}(m_{12}) + E_3^{12}(m_{12})\right)^2 - \left(\sqrt{E_2^{12}(m_{12})^2 - m_2^2} - \sqrt{E_3^{12}(m_{12})^2 - m_3^2}\right)^2. \tag{5}$$

where

$$E_2^{12}(m_{12}) = \frac{m_{12}^2 + m_2^2 - m_1^2}{2m_{12}}, \quad E_3^{12}(m_{12}) = \frac{m_B^2 - m_{12}^2 + m_3^2}{2m_{12}} \tag{6}$$

are the energies of particle 2 and 3 in the 12 rest frame, and

$$p_2^* = \sqrt{E_2^{12}(m_{12})^2 - m_2^2}, \quad p_3^* = \sqrt{E_3^{12}(m_{12})^2 - m_3^2} \tag{7}$$

are the corresponding momenta.
The region of kinematically allowed phase space described by these constraints is shown in Figure 1.

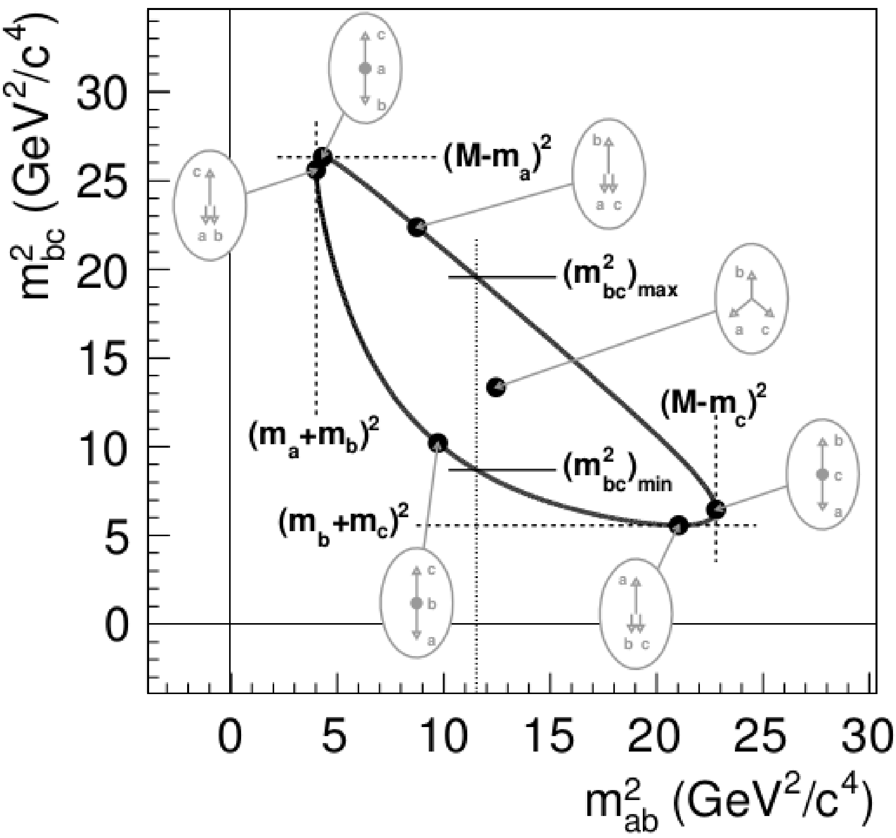

Figure 1: Kinematic boundaries of the three-body decay phase space (ref the physics of the B Factories).

Resonances

-missing-

2.3.3 Partial-Wave Expansions and Isobar Formalism

The Dalitz plot is typically dominated by resonant quasi-two-body contributions along the edges. Therefore, a first-order approximation is to regard the three-body decay as a coherent sum of quasi-two-body decays. For three-body decays of a spin-zero particle with pseudoscalar final-state particles the decay amplitude $\mathscr{A}(m^2_{12}, m^2_{23})$, is described by a coherent sum of two-body amplitudes and a "nonresonant" contribution:

$$\mathscr{A}(m) = \sum_r a_r e^{i\phi_r} \mathscr{A}_r(m) + a_{NR} e^{i\phi_{NR}} \mathscr{A}_{NR}(m) \tag{8}$$

where $m \equiv (m_{12}^2, m_{23}^2)$. The parameters a_r and ϕ_r are respectively the magnitude and phase of the amplitude for component r; and a_{NR} and ϕ_{NR} are of the component NR.

In isobar formalism, the function $\mathscr{A}_r$ describes the decay through a single intermediate resonance r and takes the form

$$\mathscr{A}_r = F_p \times F_r \times T_r \times W_r \tag{9}$$

where $T_r \times W_r$ is the resonance propagator. T_r is the dynamical function for the resonance r, while W_r describes the angular distribution of the decay. F_P and F_r are the transition form factors of the parent particle and resonance, respectively.

The isobar formalism (or isobar model) is so-called because it was first used to describe pion-nucleon, nucleon nucleon, and antinucleon-nucleon interactions (Sternheimer and Lindenbaum, 1961). In such reactions the intermediate resonances are isobars of a particular nuclear state. The isobar model was later generalized to any three-body final state (Herndon, Soding, and Cashmore, 1975).

2.4 Dalitz Plot Analysis of $B^0 \to K^+\pi^-\pi^0$

In our analysis of the $B^0 \to K^+\pi^-\pi^0$ decay, we choose the particle 1, 2 and 3 as K^+, π^-, and π^0, respectively. And the squared invariant masses then is described by $m_{12}^2 \equiv m_{K^+\pi^-}^2$, $m_{13}^2 \equiv m_{K^+\pi^0}^2$ and $m_{23}^2 \equiv m_{\pi^-\pi^0}^2$ and we write the amplitude as

$$\mathscr{A}(m_{12}^2, m_{23}^2) = \sum_i c_i \psi_i(m_{12}^2, m_{23}^2) \tag{10}$$

where the sum runs over all included resonances described by functions $\psi_i(m_{12}^2, m_{23}^2)$. The parameters c_i are complex valued and encode the the magnitude r_i and phase ϕ_i of the resonance. The magnitude describes the "strength" of a resonance and the phase difference between two resonances determines how they interfere (constructively or destructively). We normalize the functions $\psi_i(m_{12}^2, m_{23}^2)$ over the Dalitz plane such that

$$\iint_{DP} \left|\psi_i(m_{12}^2, m_{23}^2)\right|^2 dm_{12}^2 dm_{23}^2 = 1. \tag{11}$$

2.4.1 Breakdown of the Parameters

The functions describing the resonances, ψ_i, can be decomposed into four functions

$$\psi_i(m_{12}^2, m_{23}^2) = L_i(m_{12}^2) \times T_i(m_{12}^2, m_{23}^2) \times B_{res,i}(m_{12}^2) \times B_{B^0,i}(m_{12}^2), \tag{12}$$

with $L_i(m_{12}^2)$ is the part describing the mass dependence, $T_i(m_{12}^2, m_{23}^2)$ the Angular dependence, and $B_{res,i}(m_{12}^2)$, ${}_{B^0,i}(m_{12}^2)$ are the parts describing the barrier factors.

Angular Dependence of the Resonance

The angular dependence, Wr in eq 9, is described using either Zemach tensors (Zemach, 1964, 1965), or the helicity formalism (Bonvicini et al.,2008; Jacob and Wick, 1959). Here we use the Zemach formalism and the describe the angular dependence with $T(m^2_{K^+\pi^-}, m^2_{\pi^-\pi^0})$. The Zemach tensors for a spin-J resonance in system (12) is given as:

$$
\begin{aligned}
J=0: \quad & T(m^2_{12}, m^2_{23}) = 1, \\
J=1: \quad & T(m^2_{12}, m^2_{23}) = -2\,|\vec{p}|\,|\vec{q}|\cos\theta_{12} = \\
& \qquad = m^2_{13} - m^2_{23} - \frac{(m^2_P - m^2_3)(m^2_1 - m^2_2)}{m^2_{12}}, \\
J=2: \quad & T(m^2_{12}, m^2_{23}) = \frac{4}{3}\left[3(|\vec{p}|^2\,|\vec{q}|^2\cos^2\theta_{12} - (|\vec{p}|\,|\vec{q}|)^2\right] = \\
& \qquad = \left[m^2_{23} - m^2_{13} + \frac{(m^2_P - m^2_3)(m^2_1 - m^2_2)}{m^2_{12}}\right]^2 - \\
& \qquad - \frac{1}{3}\left[m^2_{12} - 2m^2_P - 2m^2_3 + \frac{(m^2_P - m^2_3)^2}{m^2_{12}}\right] \times \\
& \qquad \times \left[m^2_{12} - 2m^2_1 - 2m^2_2 + \frac{(m^2_1 - m^2_2)^2}{m^2_{12}}\right]
\end{aligned}
\tag{13}
$$

$\vec{p}$ is the momentum of the bachelor particle, i.e. π^0, for a resonance in system (12), and $\vec{q}$ is the momentum of one of the daughters of the resonance. Both of them are evaluated in the rest-frame of the resonance. θ_{12} is the angle between $\vec{p}$ and $\vec{q}$.

Angular Momentum Barrier Factors

In the description of the resonance, we need to include a term accounting for the additional energy needed to create the angular momentum $L = J$ between the decay products of the two-body decay of a spin-J resonance in order to conserve angular momentum. Therefore the expression we use depend on the spin J of the intermediate resonance. We use the Blatt-Weisskopf barrier factors $B_{res}(m^2_{12})$, for consequent the intermediate resonance decaying to the remaining two of the final state particles, and $B_{B^0}(m^2_{12})$, for B^0 decaying to the intermediate resonance and the bachelor particle, as the orbital angular momentum compensation factors where for a spin-0 resonance $L = 0$ it reads $B = 1$. The Blatt-Weisskopf parameterization is formulated as:

$$
\begin{aligned}
J=0: \quad & B(m^2_{12}) = 1, \\
J=1: \quad & B(m^2_{12}) = \sqrt{\frac{1 + R^2\,|\vec{q}_0|^2}{1 + R^2\,|\vec{q}(m^2_{12})|^2}}, \\
J=2: \quad & B(m^2_{12}) = \sqrt{\frac{9 + 3R^2\,|\vec{q}_0|^2 + R^4\,|\vec{q}_0|^4}{9 + 3R^2\,|\vec{q}(m^2_{12})|^2 + R^4\,|\vec{q}(m^2_{12})|^4}},
\end{aligned}
\tag{14}
$$

where R is the radius of the interaction assumed that describes the meson resonance. We evaluate the B_{res} at the resonance rest-frame where $|\vec{q}(m^2_{12})|$ is the two-body breakup momentum of the particles 1 and 2 in the resonance rest frame (K^* rest frame / isobar frame) and $|\vec{q}_0|$ is the $|\vec{q}(m_{12}^2)|$ at the nominal mass of the resonance i.e. $|\vec{q}_0| = |\vec{q}(m_{res}^2)|$. $|\vec{q}(m_{12}^2)|$, the two-body breakup momentum for a decay $P \rightarrow a + b$, is formulated as

$$|\vec{q}|\,(m_P^2) = \frac{(m_P^2 - (m_a + m_b)^2)(m_P^2 - (m_a - m_b)^2)}{2m_P} \tag{15}$$

For B_{B^0} we compare two different formulations: one at the resonance rest-frame where $|\vec{q}(m_{12}^2)|$ is given by the momentum of the bachelor particle π^0 and $|\vec{q}_0|$ is the bachelor momentum (in isobar frame) at the nominal mass of the resonance, and the other at the B^0 rest frame where $|\vec{q}(m_{12}^2)|$ is the two-body breakup momentum of the bachelor particle and the 2-particle system.

Mass-dependent Line-shapes

The functions $L(m_{12}^2)$ are called the line-shapes and describe the mass dependence of the resonance. We use for the K^* resonance. The Breit-Wigner line-shape for a resonance in system (12) is given by

$$L(m_{12}^2) = \frac{m_0\Gamma_0}{m_0^2 - m_{12}^2 - im_0\Gamma(m_{12})}, \tag{16}$$

where m_0 is the the nominal mass and Γ_0 the width of the resonance. $\Gamma(m_{12}^2)$ is the mass dependent width and it's given by

$$\Gamma(m_{12}^2) = \Gamma_0 \frac{|\vec{q}(m_{12}^2)|^{2J+1}}{|\vec{q}_0|^{2J+1}} \frac{m_0}{m_{12}} \frac{B^2(m_{12}^2)}{B^2(m_0^2)} \tag{17}$$

where B are the barrier factors described in equation 14.

3 Analysis of Amplitude Models

In this section, we will investigate how each parameter and the choice of reference frames affect the intensity of $B^0 \to K^+\pi^-\pi^0$ decay, since intensity is the the physical quantity we can measure. As the momenta are different in different reference frames, we compared the spin dependent Zemach (shown in eq.13) and Blatt-Weisskopf (shown in eq.14) functions in 2 different reference frames: B rest frame and the isobar rest frame; since they can be expressed in terms of momenta as well instead of the masses. The reference frames and the corresponding momenta are illustrated in Figure 2.

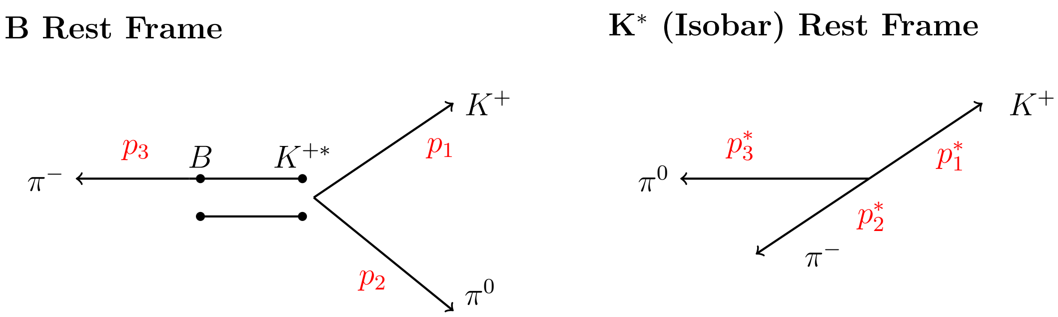

Figure 2: Decay diagrams in the B rest frame and K* rest frame.

3.1 Different Factors in Amplitude Model

Spin Dependence

We started with looking at $T_i(m_{12}^2, m_{23}^2)$, the Zemach tensors encapsulating the spin dependence of the amplitude of resonance, which relate to mass/energy. i. There are multiple formalisms used to describe the function T_i, it can alternatively be expressed in terms of $\vec{q}$ two-body breakup momentum of the B and the 2-particle system and $\vec{p}$, momentum of the bachelor particle in chosen reference frame.
Similarly $B_i(m_{12}^2)$, the spin dependent Blatt-Weisskopf angular momentum barrier factors, can also be written in terms of different momenta. The selections for the barrier factors is explained in section 2.4.1, Angular Momentum Barrier Factors.
We are interested in how different momenta contribute to the calculation of the amplitude $\mathscr{A}_r$. However, for experiments it is preferred to use the intensity instead of the amplitude since unlike the amplitude, which can be complex valued, the intensity the physical quantity we can measure; and it is given by

$$I_i = |\mathscr{A}_i|^2 = L_i^2 \times T_i^2 \times B_{res,\,i}^2 \times B_{B^0,\,i}^2. \tag{18}$$

Therefore we made the plots for the squared form of the spin dependent functions. The plots for the spin 1 case is shown in Figure 3. The Figure 3 consists of two graphs both in which the blue, continuous line depicts both spin dependent energy and the barrier factor of B^0 in B^0 rest frame; the orange, dashed line depicts the spin dependent energy at isobar frame with spin dependent the barrier factor of B^0 in B^0 rest frame; and the green, dotted line depicts both the spin dependent energy and barrier factor of B^0 in isobar frame. The difference between the graphs at the right and at the left is that the one on the right has the rescaled version of the blue line where its maximum is scaled to the maximum of the green one with

$$blue_{rescaled} = blue \times \frac{green_{max}}{blue_{max}}, \tag{19}$$

as well as the orange one with

$$orange_{rescaled} = orange \times \frac{green_{max}}{orange_{max}}, \tag{20}$$

while the green lines are the same in both graphs.
Also, bear in mind that contribution from the barrier factor for resonance is always calculated at resonance rest frame throughout this analysis.

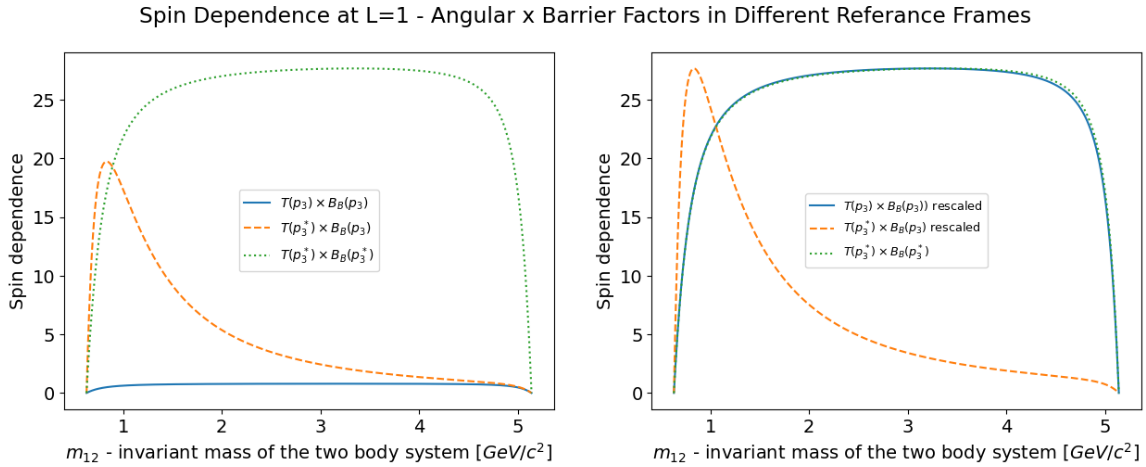

Figure 3: Plot of $T^2(\vec{p},\vec{q}) \times B^2_{res}(\vec{p'},\vec{q'}) \times B^2_{B^0}(\vec{p''},\vec{q''})$ parametrized by different momenta against the invariant mass of the two body system for L = 1. (left) And the same plot when the maximum of the first and the second lines rescaled to maximum of the third.(right)

In Figure 3, looking at the rescaled version, we see that the spin dependent energy (squared) multiplied with the angular momentum barrier factor for the B^0 decay (squared) give somewhat similar shapes for the blue and the green lines, which depict the parametrizations made using the same reference frame for both Zemach and Blatt-Weisskopf functions. The blue line illustrates both Zemach and Blatt-Weisskopf functions for spin 1 calculated in B^0 rest frame and green line illustrates both Zemach and Blatt-Weisskopf functions for spin 1 calculated in the isobar frame. Meanwhile, the orange line illustrating the Zemach function in isobar and Blatt-Weisskopf in B^0 rest frame differ significantly from both blue and green lines. For the orange line's parametrization, the spin dependent contribution increases faster at small invariant masses of the two body system, peaking shortly after it gradually decreases, the slower as the invariant mass gets bigger, except near the upper limit of the invariant mass of the two body system. However, for both the blue and green line's parametrization, while it also increases faster at small invariant masses, then it follows a rather plateau shape until when it gets close to the upper limit of the invariant mass rapidly decreasing thereafter.

One interpretation of this observation is that when we choose the isobar frame formulation for the Zemach functions but not adjust formulation of the barrier factors to the same reference frame, we get a different behavior of the spin dependence as opposed to the behaviour we get when we use the formulation from the same reference frame for all spin dependent functions regardless of if all are made in B^0 rest frame or isobar frame. The choice of the reference frame seems to only slightly affect the contributions from the spin dependent parts of the amplitude if we choose a consistent reference formulation for all spin dependent functions.
Next we added the contributions from the mass dependent lineshape (squared) and the phase space (as a correction factor). What we get then is the intensity for a resonance r, I_r, which is shown in Figure 4. The resonance we chose for this case is K^{+*} described by the Breit-Wigner lineshape. The Figure 4 consists of two graphs both in which the blue, continuous line depicts the intensity described by both spin dependence and the barrier factor of B^0 in B^0 rest frame; the orange, dashed line depicts the intensity described by the spin dependence formulated at resonance rest frame and the the barrier factor of B^0 in B^0 rest frame; and the green, dotted line depicts the intensity described by both spin dependence and the barrier factor of B^0 calculated in resonance rest frame.

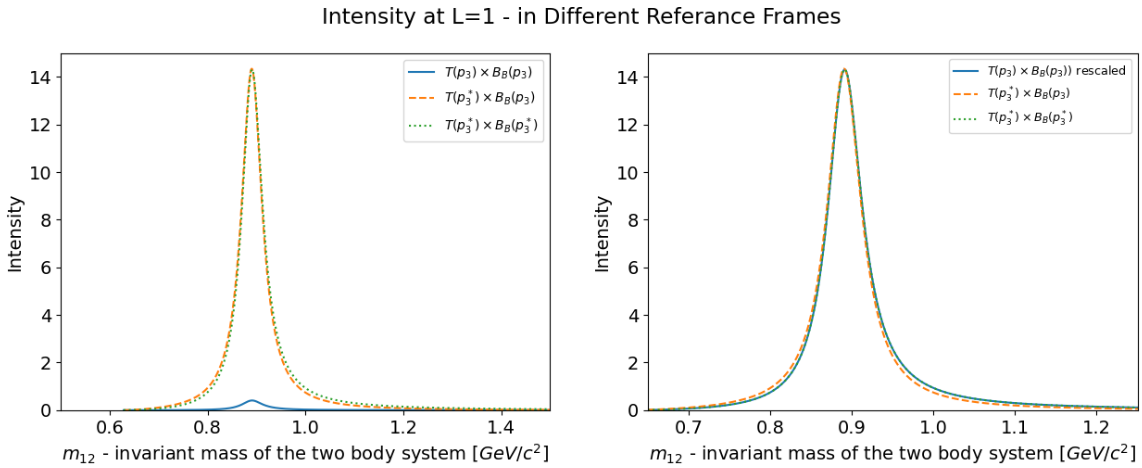

Figure 4: Plot of Intensity corrected with the phase space factor, given by $T^2(\vec{p},\vec{q}) \times B^2_{res}(\vec{p'},\vec{q'}) \times B^2_{B^0}(\vec{p''},\vec{q''}) \times L^2_{BW}(m^2_{12}) \times p^*_1 \times p_3$ parametrized by different momenta against the invariant mass of the two body system for L = 1.(left) And the same plot when the maximum of first line rescaled to maximum of the second.(right)

When we look at the the right (rescaled) graph of Figure 4 , we see that unlike the case in Figure 3, all three parametrization give in Figure 4 describe very similar shapes, with blue and green lines being almost identical and the orange displaying a slight shift towards left.
From this graph, we conclude that the impact of the contributions from the spin dependent functions formulated in different reference frames is diminished when we calculate the intensity. We attribute this to the narrowness of the resonance.

The Figures 5 and 6 replicate the parametrizations illustrated at Figures 3 and 4, respectively, for the spin 2 case. Additionally, the resonance chosen in these graphs is the K_2^{+*}

instead of K^{+*} .

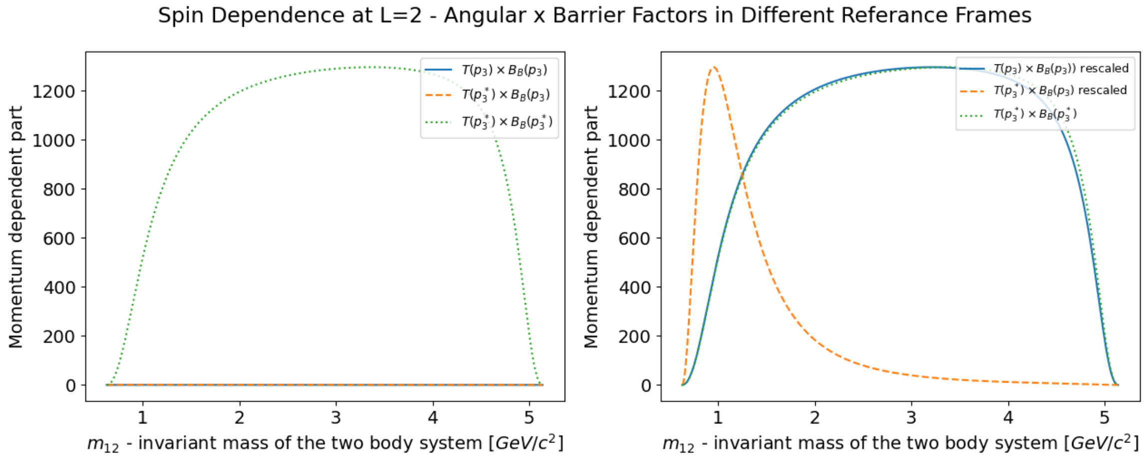

Figure 5: Plot of $T^2(\vec{p}, \vec{q}) \times B^2_{res}(\vec{p'}, \vec{q'}) \times B^2_{B^0}(\vec{p''}, \vec{q''})$ parametrized by different momenta against the invariant mass of the two body system for L = 2. (left) And the same plot when the maximum of first line rescaled to maximum of the second.(right)

In Figure 5, we observe an outcome similar to the one in Figure 3. Except, this time it is easier to tell the blue line and green line apart. The importance of the reference frame choice is still significantly low, but this observation does tell us for other resonances, the spin dependent contributions might differ for isobar and B^0 rest frame formulations even when they are done 'consistently', and that the difference between using both momenta from the isobar or the B^0 rest frame is larger than in the spin 1 case, demonstrating that the effect becomes larger with larger spin. When we compare the case where the momenta where chosen from different reference frames for the two different spin cases, we see that difference is even starker for the higher spin. While in the spin 1 case the approximations made for invariant two body mass below about 0.8 GeV/c^2 give a similar description for all of the parametrizations, the discrepancy between the consistent and inconsistent reference frame parametrizations is still noticeable for the spin 2 case.

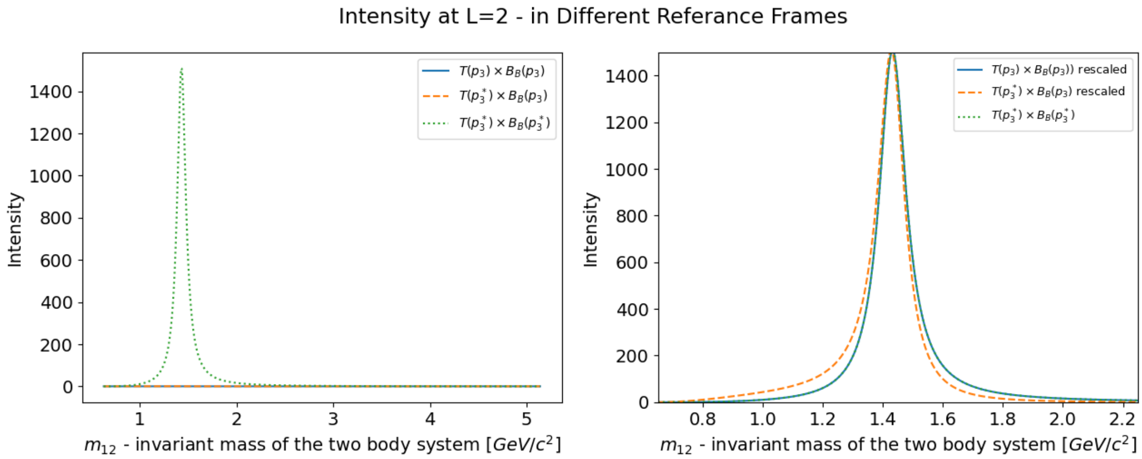

Figure 6: Plot of Intensity given by $T^2(\vec{p},\vec{q}) \times B^2_{res}(\vec{p'},\vec{q'}) \times B^2_{B^0}(\vec{p''},\vec{q''}) \times L^2_{BW}(m^2_{12})$ parametrized by different momenta against the invariant mass of the two body system for L = 2.(left) And the same plot when the maximum of first line rescaled to maximum of the second.(right)

In Figure 6 we see that while the blue and green lines are still almost indistinguishable but the shift of the orange line we saw in figure 4 becomes even larger towards the tails. From this, we observe that the impact of the contributions from the spin dependent functions formulated in different reference frames is again reduced significantly when we calculate the intensity, however the difference between the intensities formulated with 'consistent' and 'inconsistent' reference frame formulations of spin dependent functions becomes larger due to the wider resonance width. And this difference becomes also larger with larger spin. All in all we conclude that one must be careful when choosing the reference frame for the parametrizations of the amplitude, especially in the case of wide resonances. And once the the parametrization choice for one of the spin dependent functions is made, it is highly advisable to continue with same reference frame choice for the other spin dependent functions, remembering that as long as they are consistent, the difference in the amplitude between both choices is very small.

4 Analyzing the Data

The next step after after completing the amplitude model is to analyze the observed data to uncover the physics of the decay. However, to avoid any bias towards the results, we need settle on every aspect of the analysis. This includes 'tests' done using simulated data for possible problems and the computation methods we want to use. Even the the choices for the packages and frameworks is better to be finalized by this step. Only after we understand and set on what we are doing we should start analyzing the real data. For this reason, what we next to is to evaluate the fitter we use in our analysis.

The Data

The data we use for the fits is a Monte-Carlo generated, signal only data that doesn't include any background. More specifically, we use simulated $B^0 \to K^+\pi^-\pi^0$ decay data that is generated according to the BABAR model. (cite!!)

The Fit Model

We fit the our Amplitude model to the data in order to determine complex couplings corresponding to the modeled resonances. , c_i, are the fit parameters that we want to determine.

4.1 The Fitter

We perform an unbinned maximum-likelihood fit using the zfit package(cite!!). The fitter's primary objective is to optimize the parameters of a given probability density function (PDF) to best describe the data. In our analysis, it minimizes the negative log likelihood. (A. Huschle, J. Pata, and M. Erdmann, *zfit: scalable Pythonic fitting*, https://github.com/zfit/zfit.)

4.1.1 Start-Parameter Dependence

Given how the fitter works, we need to define a set of start parameters. Due to the nature of the fitter, one thing we should be careful of is its consistency. While we have a range of prediction for the coefficients and we can choose to tell the fitter to start from there, first we would need to know if our choice would affect the results. Does the fitter always find the same minimum, and how do different minima affect the parameters we get from the fitter? Answering these questions is crucial for evaluating the fitter's consistency, hence we studied how different start parameters affect our results.

First we looked at whether the fitter finds the same minimum if it starts the optimization with different start values. To see if there is a dependence on the choice of start parameters, we performed multiple fits with different start parameter values selected randomly. To randomize the parameters we used a randomizing function from zfit, the fit package we have been using for the fit. To set the limit of the parameters to a certain chosen value we use our start parameter model.

We generally used 100 iterations of fit attempts to analyze the start value dependence.

We stored the resulting fit parameters, i.e. couplings, and the min log likelihood of the fit for each fit attempt and made a histogram of the min log likelihood of the 100 iterations of fit attempts. The histogram is shown in Figure 7

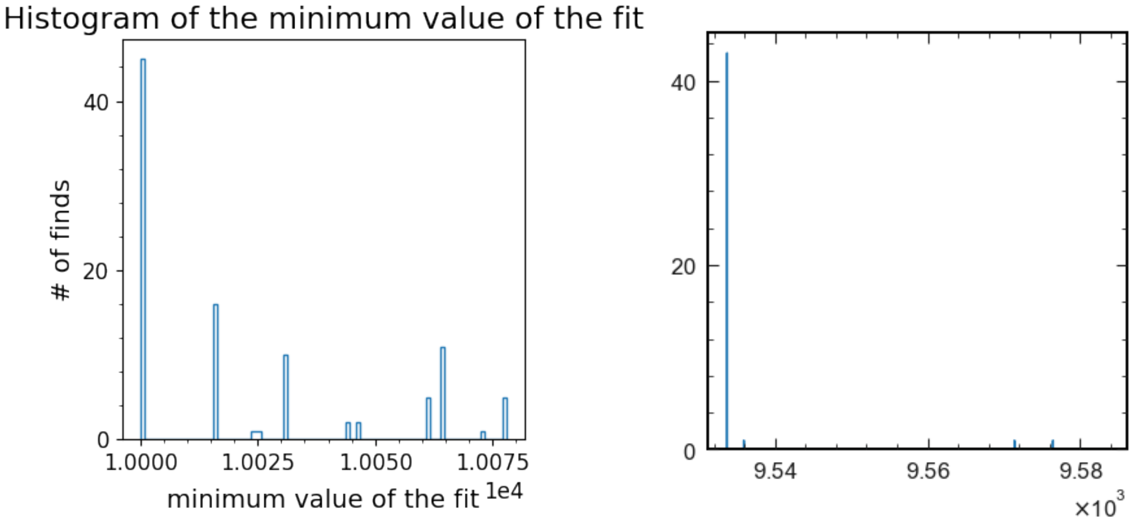

Figure 7: Histogram of the minimum log likelihood of the fitter over 100 iterations of fit attempts each with a different random start value(left), same plot zoomed in lower minimum log likelihoods(right).

We can see from the histogram in Figure 7 that the fitter seems to find the same minimum 45% of the time. As the fitter doesn't always find the same minimum, we shouldn't use set values. but it can find it in a sufficient amount of fit attempts. Our method of circumventing this issue was to taking the best of 10 attempts. As it 'correctly' finds the minimum half of the time, performing 10 fits should be statistically sufficient without increasing the computation cost too much.
Next, we looked at whether the fitter found the couplings consistently. Using the coupling values we stored, we made a scatter plot of the real part and the imaginary part of the couplings for each of the seven parameters, which shows the fit result for the coupling values, real and imaginary parts separated, with the corresponding minimum log likelihood of that fit. The values for the first coupling is shown in Figure 8 as an example.

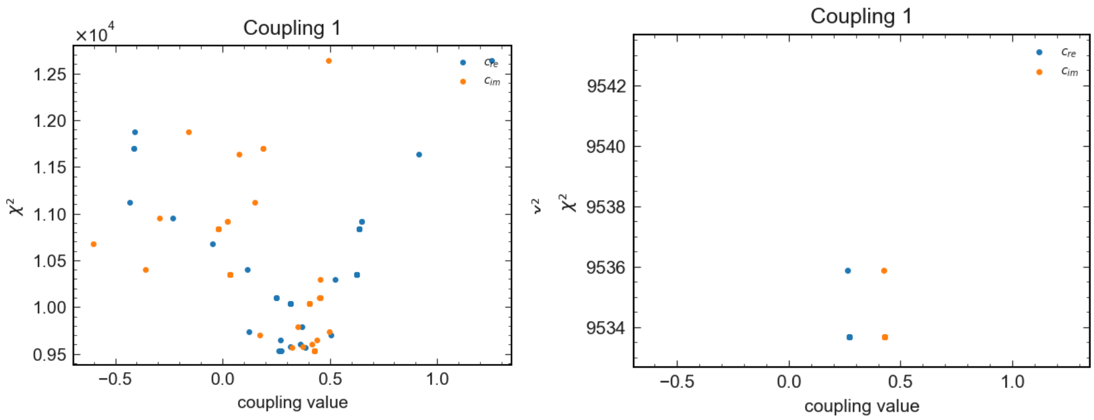

Figure 8: Fit result (100 fit attempts)for the coupling 1 values, real and imaginary parts separated, with the corresponding minimum log likelihood of that fit(left), same plot zoomed in lower minimum log likelihoods(right).

While the fitted values of the parameters seems to be scattered for the general fit, we see that they are consistent for fits with the lowest minima. It can be misleading to interpret the graphs shown in Figure 8 without taking the graphs in Figure 7 into account, as at first glance it seems like the fitter finds various values for the couplings in different fit attempts. However, we are not interested in all fit attempts, but the ones with lowest minima. Again, we may mistakenly think that there aren't many couplings for the low minima, but we already know this is not the case! We already concluded from the histograms in Figure 7 that the fit result provided are from the lowest minima half of the time. And this doesn't contradict with our results from Figure 8 since Figure 8 doesn't actually tell us how many couplings there are in a shown coupling value, but rather which values for the couplings are found in a fit with what minimum log likelihood. So combining our observation from both graphs, we can deducted that the result we have from the right graph in Figure 8 is very good! For all 40 of the lowest minima we get the indistinguishable values. This deduction once again shows us the importance of the start value dependence. We cannot be sure from only 1 fit attempt if get meaningful and consistent results for our analysis, but we find that can obtain them more confidently, if we take the best of 10 fit attempt done with randomized the start values.

5 Conclusion

5.1 summary

A notable result of the analysis done during this study, which examines the amplitude models of the $B^0 \to K^+\pi^-\pi^0$ decay using the Dalitz plot formalism, is the demonstration of the behavior of spin-dependent functions evaluated in different reference frames: B rest frame, and isobar rest frame. We find that consistent reference frame parametrizations yield similar behaviors. And the influence of spin-dependent functions diminishes when focusing on intensity calculations. We conculude that the reference frame choices have minimal impact, especially for narrow resonances, in contrast, discrepancies in amplitude become more pronounced with increasing resonance width and higher spin states.
Consistent minima were achieved in approximately 45 of the fits. To mitigate issues related to the dependence of fit results on initial parameter choices, it is recommended to perform multiple fitting attempts with randomized start values and select the best-performing fit from these attempts to ensures more reliable results.

The sources used in this analysis are not completely stated above but thay will be included in the bibliography. [3] [4] [5] [6] [7]

References

[1] Makoto Kobayashi and Toshihide Maskawa. “CP-Violation in the Renormalizable Theory of Weak Interaction”. *Progress of Theoretical Physics* 49.2 (Feb. 1973), pp. 652–657. ISSN: 0033-068X. DOI: 10.1143/ptp.49.652.

[2] S. W. Herb et al. “Observation of a Dimuon Resonance at 9.5-GeV in 400-GeV Proton-Nucleus Collisions”. *Phys. Rev. Lett.* 39 (1977), pp. 252–255. DOI: 10.1103/PhysRevLett.39.252.

[3] E. Kou et al. “The Belle II Physics Book”. *Prog Theor Exp Phys (2019)* 2019.12 (Dec. 2018). DOI: 10.1093/ptep/ptz106. arXiv: 1808.10567 [hep-ex].

[4] Matthias Neubert. *Introduction to B Physics.* 2000. arXiv: hep-ph/0001334 [hep-ph]. URL: https://arxiv.org/abs/hep-ph/0001334.

[5] A. J. Bevan et al. “The Physics of the B Factories”. *The European Physical Journal C* 74.11 (Nov. 2014). ISSN: 1434-6052. DOI: 10.1140/epjc/s10052-014-3026-9.

[6] Vanamali Shastry, Enrico Trotti, and Francesco Giacosa. “Constraints imposed by the partial wave amplitudes on the decays of ¡mml:math xmlns:mml=”http://www.w3.org/1998/Math/ display=”inline”¿¡mml:mi¿J¡/mml:mi¿¡mml:mo¿=¡/mml:mo¿¡mml:mn¿1¡/mml:mn¿¡/mml:math¿ , 2 mesons”. *Physical Review D* 105.5 (Mar. 2022). ISSN: 2470-0029. DOI: 10.1103/physrevd.105.054022. URL: http://dx.doi.org/10.1103/PhysRevD.105.054022.

[7] Charles Zemach. “Use of Angular-Momentum Tensors”. *Phys. Rev.* 140 (1B 1965), B97–B108. DOI: 10.1103/PhysRev.140.B97. URL: https://link.aps.org/doi/10.1103/PhysRev.140.B97.

Declaration of authorship

Declaration: I hereby declare that this thesis is my own work, and that I have not used any sources and aids other than those stated in the thesis.

Location, date Munich, 05.02.2025

Name Ceren Ay